



Letters to the Editor

## Intensity and profile manifestation of resonant Raman behavior of carbon nanotubes

P.H. Tan<sup>a,\*</sup>, C.Y. Hu<sup>a</sup>, F. Li<sup>b</sup>, S. Bai<sup>b</sup>, P.X. Hou<sup>b</sup>, H.M. Cheng<sup>b</sup><sup>a</sup>National Laboratory for Superlattices and Microstructures, P.O. Box 912, Beijing 100083, China<sup>b</sup>Institute of Metal Research, Chinese Academy of Sciences, Shenyang 110015, China

Received 20 December 2000; accepted 26 August 2001

*Keywords:* A. Carbon nanotubes; C. Raman spectroscopy*PACS:* 63.22.+m; 78.30.Na; 71.20.Tx

Since the discovery of multiple-walled carbon nanotubes (MWNTs) and single-walled carbon nanotubes (SWNTs) [1,2], much attention has been paid to both fundamental and applied research on carbon nanotubes [3]. Raman scattering is a simple but powerful technique to analyze MWNT and SWNT products [4–6]. The C–C stretching mode (G) of MWNTs is very similar to that of graphite [5], while that of SWNTs shows multiply splitting peaks because of the size-dependent zone-folding effect of SWNTs [4,7]. However, the disorder slightly influences the frequency of G mode in graphite materials, and the frequency of G mode in the ion-implanted graphite can shift to higher values up to  $1595\text{ cm}^{-1}$  [8]. The G mode of MWNT made by the catalytic method with high degree of disorder also shifts to  $1600\text{ cm}^{-1}$  [5], which is close to the frequency of C–C stretching mode in SWNT. Therefore, in some cases, it is difficult to distinguish SWNT from MWNT by peak positions of their C–C stretching modes. Here, we report a way to distinguish SWNT from MWNT by studying Raman intensities of C–C stretching modes under the same experimental condition. Raman spectra of SWNTs are strongly dependent on the laser excitation [6,9] as well as on the sample spot [10] because of diameter-selective resonant Raman effect of SWNTs. Different resonant behaviors of Raman spectra are found between Stokes and anti-Stokes regions of C–C stretching modes by comparing the profiles of C–C stretching modes between Stokes and anti-Stokes sides [11,12]. In this paper, we find that the Raman intensity and profile of C–C stretching modes of SWNTs are strongly dependent on sample spot. Raman spectra of C–C stretching modes also

exhibit different intensities and asymmetric profiles between their Stokes and anti-Stokes scattering components. We conclude that these results are originated from the different resonant behaviors of the observed SWNTs with different diameters by analyzing the resonant behavior of the radial breathing modes (RBMs) of SWNTs.

The SWNT sample was prepared by the catalytic hydrocarbon decomposition method [13]. The experimental parameters used in the preparation of MWNTs were different but the processes were very similar to each other. Raman-scattering spectra were recorded by the Dilor SuperLabram with a typical spectral resolution of  $1.0\text{ cm}^{-1}$  in the measured frequency region. Samples are excited using the  $632.8\text{ nm}$  line of a He–Ne laser with a spatial resolution of less than  $2\text{ }\mu\text{m}$ . The sample is kept at room temperature by using the low laser power of  $40\text{ }\mu\text{W}$ .

Fig. 1 shows Raman spectra of pyrolytic graphite, MWNTs and SWNTs in the region between  $1200$  and  $1800\text{ cm}^{-1}$  under the same experimental conditions. The spectra of SWNTs at two different sample spots are given. For MWNT, there are three main peaks located at  $1332$ ,  $1585$  and  $1620\text{ cm}^{-1}$ , which are designated as disorder-induced (D) mode, C–C stretching (G) mode and disorder-induced (D') mode, respectively, similar to those of pyrolytic graphite. The detailed Raman modes of SWNT are shown in Fig. 2.

As shown in Fig. 1, the Raman intensity of C–C stretching modes of SWNTs is found to be much stronger than that of MWNTs. For graphite materials, the C–C stretching modes are determined by very local properties with minor perturbation from the geometry and their intensities are determined by the number of carbon atoms per unit volume [14]. For a MWNT, its outer diameter

\*Corresponding author.

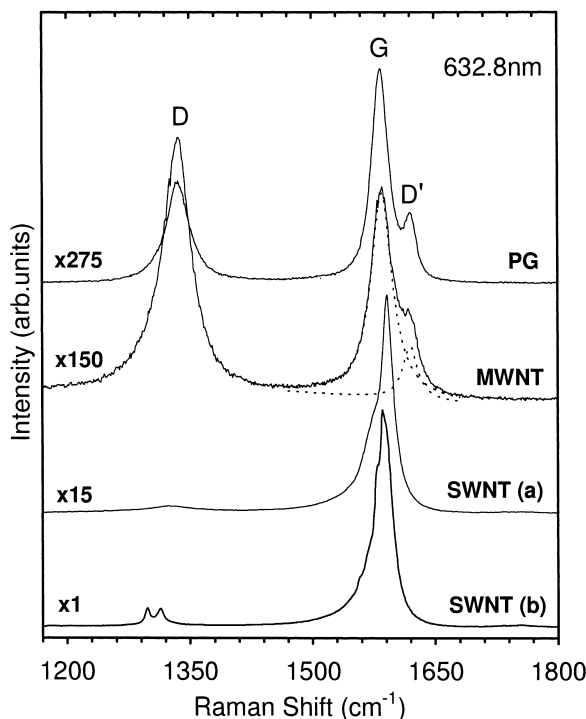


Fig. 1. Raman bands associated with the disorder-induced modes and C–C stretching modes of pyrolytic graphite, MWNTs and SWNTs (measured at two sample positions (a) and (b)) obtained under the same experimental conditions.

usually lies in the range of 10 to 20 nm, and an inner space of  $\sim 3$  nm in diameter exists in a tubule. The inter-wall spacing of a MWNT is very close to the interlayer spacing of a graphite lattice. Thus, the number of carbon atoms per unit volume in MWNT sample is close to that in graphite. However, considering that the SWNT sample usually contains many bundles of SWNT arranged in a triangular lattice (with lattice constant  $a_{\text{tri}}$ ), the ratio of carbon atoms between SWNT and graphite lattice in the same volume can be roughly estimated to be  $2\pi a_{c\text{-axis}} d_t / [\sqrt{3} a_{\text{tri}}^2]$ , where  $a_{c\text{-axis}}$  and  $d_t$  are, respectively, the interlayer spacing ( $\sim 0.34$  nm) of a graphite lattice and the diameter of a SWNT. This ratio is almost equal to 0.48 for  $d_t = 1.7$  nm and  $a_{\text{tri}} = 2.1$  nm. The actual ratio is much smaller than this value because of the existence of free space between SWNT bundles. Therefore, the intensity of the C–C stretching mode of SWNT should be lower than that of MWNT except for other critical reasons. The diameter of graphene tubes of a MWNT usually varies from 3 nm to more than 20 nm and is much larger than that of SWNT, and the energy separations between spikes in the 1D electronic states are much smaller than the incident photon energy. As most of our SWNT sample covers the range of diameter from 1.0 to 2.0 nm, the quantum confined effect on the electron states of SWNTs is very remarkable and

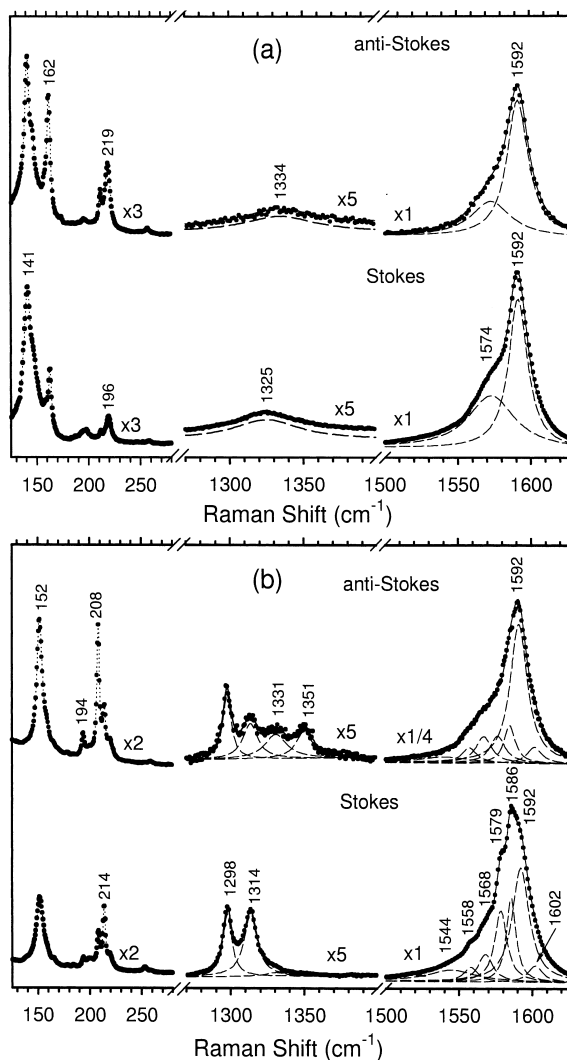


Fig. 2. Stokes (bottom) and corrected anti-Stokes (up) Raman spectra of SWNTs at the low- and high-frequency regions at two sample spots. The dashed lines represent the individual Lorentzian components, and the solid curves show the fit to the experimental results (solid circles). The Stokes and corrected anti-Stokes spectra are plotted with the same x-scale for convenience.

the energy separation between spikes for the 1D electronic density of states (DOS) of SWNTs covers a very wide range [6]. Therefore, when electronic energy separation of SWNTs is close to the energies of incident or scattered (Stokes or anti-Stokes) photons, the resonant scattering process for those particular diametric SWNTs dominates the Raman spectra of SWNTs. Thus, the strongly enhanced intensity of C–C stretching mode of SWNT results from the resonantly enhanced Raman scattering process of SWNTs with some special diameter whereas such resonant enhancement is very weak for MWNTs because of their large diameters of graphene tubes.

Fig. 1 also shows that Raman spectra of SWNTs are strongly dependent on the sample spot. The intensity of C–C stretching modes taken at spot (b) is 15 times as strong as that taken at spot (a). Fig. 2a and b, respectively, show Stokes and anti-Stokes Raman spectra of SWNTs in the low- and high-frequency regions taken at the two different sample spots (a) and (b). The anti-Stokes Raman components in the figures have been multiplied by the correction factor  $\alpha_{s/as}$  at room temperature which was defined in Eq. (1) of Ref. [10]. The Raman spectra associated with the C–C stretching modes in Fig. 2a show almost equal intensity between Stokes and anti-Stokes sides, whereas the corrected intensity of C–C stretching modes at anti-Stokes side in Fig. 2b is about four times as strong as that of the corresponding modes at Stokes side. All the results show that the observed SWNTs at spot (b) are much more strongly in resonance with the incident or scattered photons than those at spot (a). This suggests that the SWNT sample is very inhomogeneous [10]. Due to sample inhomogeneity, different sample spots exhibit different diameter distributions of SWNTs, and thus Raman spectra at different sample spots exhibit different resonantly enhanced scattering.

The frequency of RBM is only sensitive to inverse tube diameter [15] and the resonant behavior of RBMs can be used to study the resonant behavior of the observed SWNTs with some special diameters [10]. In Fig. 2a, the RBMs at 162 and 219  $\text{cm}^{-1}$  exhibit different intensities between Stokes and anti-Stokes sides whereas the 141  $\text{cm}^{-1}$  mode has almost the same intensity at Stokes and corrected anti-Stokes sides. This indicates that the observed SWNTs with the 141  $\text{cm}^{-1}$  RBM are under nonresonant conditions whereas those with the 162 and 219  $\text{cm}^{-1}$  RBMs are in resonance with the incident or scattered photons. Note that the intensity of non-resonant bands located at about 141  $\text{cm}^{-1}$  is comparable to that of other resonant RBMs. This implies that most of the observed nanotubes have diameters with RBM at about 141  $\text{cm}^{-1}$ . Thus, the Stokes and anti-Stokes spectra of C–C stretching modes exhibit a nonresonant spectral feature that Stokes and anti-Stokes C–C stretching modes show almost equal intensity.

In Fig. 2b, the intensity of many RBMs at anti-Stokes side is different from that of the corresponding modes at Stokes side, especially for the RBM group located at about 152 and 210  $\text{cm}^{-1}$ . The TEM image shows that the nanotubes in this study are self-assembled into bundles. Thus, we used the expression of  $\omega (\text{cm}^{-1}) = 254/d (\text{nm})$  to calculate the diameter of SWNTs. With the above expression, the diameter of the nanotube related to the 152- and 210- $\text{cm}^{-1}$  RBM is 1.68 and 1.21 nm, respectively. When taking the nearest-neighbor overlap integral  $\gamma_c$  as 2950 meV [9], the theoretical calculation [16] shows that the energy separation of the third pair of DOS singularities in the valence and conduction bands for semiconducting SWNTs with 152  $\text{cm}^{-1}$  RBM is about 2020 meV, and the

transition energy of the first pair of DOS singularities in metallic tubes with 210  $\text{cm}^{-1}$  RBM is about 2100 meV. These electronic transition energies of some semiconducting or metallic SWNTs with special diameters are close to those (about 2150 meV) of anti-Stokes photons of C–C stretching modes. As a result, C–C stretching modes are resonantly enhanced at the anti-Stokes side. This stronger resonant Raman scattering process of RBMs in Fig. 2b also causes the intensity of C–C stretching modes in Fig. 2b to be much stronger than that in Fig. 2a, as shown in Fig. 1, because most observed SWNTs in Fig. 2b show a stronger resonant process.

In contrast to the symmetric profile between Stokes and anti-Stokes sides of the C–C stretching modes in Fig. 2a, the Stokes and anti-Stokes spectra of the C–C stretching modes in Fig. 2b show asymmetric profiles, similar to the results reported by Brown and co-workers [11,12]. According to the structural shapes of Stokes and anti-Stokes components, at least seven different peaks, located at 1544, 1558, 1568, 1579, 1586, 1592 and 1602  $\text{cm}^{-1}$ , are necessary to give a good fit to the experimental data at both Stokes and anti-Stokes sides. These modes exhibit different intensity relative to 1592  $\text{cm}^{-1}$  between Stokes and anti-Stokes sides. Raman bands (1298, 1314, 1331 and 1351  $\text{cm}^{-1}$ ) associated with disorder-induced modes in the region 1260–1400  $\text{cm}^{-1}$  also exhibit asymmetric profiles between the Stokes and anti-Stokes components. The asymmetric profiles of spectra of SWNTs between Stokes and anti-Stokes sides can be attributed to the diameter-dependent resonant Raman effect [11,12]. RBMs in Fig. 2b cover a wider diameter distribution from 150 to 230  $\text{cm}^{-1}$  and show different resonantly enhanced process between Stokes and anti-Stokes sides. This suggests that the electronic transition energies of the different diametric nanotubes have different energy shifts relative to the scattered photons. The closer the electronic transition of SWNTs with special diameter to the energy of anti-Stokes scattered photon is, the stronger the intensity of C–C stretching modes associated with nanotubes at anti-Stokes side. The different enhanced process of SWNTs causes the intensity redistribution of those unresolved-multiple-splitting stretching modes between Stokes and anti-Stokes sides relative to 1592  $\text{cm}^{-1}$  mode, and further, the asymmetric profiles of C–C stretching modes between Stokes and anti-Stokes signals.

In conclusion, resonant Raman behaviors of SWNTs and MWNTs are studied by analyzing the intensities and profiles of their C–C stretching modes. The spectra of the C–C stretching modes exhibit different intensities and asymmetric profiles between their Stokes and corrected anti-Stokes scattering components. Spectra taken at some other sample spots show almost equal intensities and symmetric profiles. By analyzing the resonant behavior of radial breathing modes, we show that the different intensities and profiles of C–C stretching modes between different sample spots and between Stokes and anti-Stokes

spectra result from the different resonant behaviors of observed SWNTs with different diameters. Moreover, the Raman intensity of C–C stretching modes of SWNTs is found to be much stronger than of MWNTs. The results indicate that one can distinguish SWNT from MWNT by the intensity analysis of their C–C stretching modes.

## References

- [1] Iijima S. *Nature* 1991;354:56–8.
- [2] Iijima S, Ichihashi T. *Nature* 1993;363(6430):603–5.
- [3] Dresselhaus MS, Dresselhaus G, Eklund PC. *Science of fullerenes and carbon nanotubes*. San Diego: Academic, 1996.
- [4] Eklund PC, Holden JM, Jishi RA. *Carbon* 1995;33(7):959–72.
- [5] Tan PH, Zhang SL, Yue KT, Huang FM et al. *J Raman Spectrosc* 1997;28(5):369–72.
- [6] Rao AM, Richter E, Bandow S, Chase B et al. *Science* 1997;275(5297):187–91.
- [7] Kasuya A, Sasaki Y, Saito Y, Tohji K, Nishina Y. *Phys Rev Lett* 1997;78(23):4434–7.
- [8] Elman BS, Dresselhaus MS, Dresselhaus G, Maby EW, Mazurek H. *Phys Rev B* 1981;24(2):1027–34.
- [9] Pimenta MA, Marucci A, Empedocles SA, Bawendi MG et al. *Phys Rev B* 1998;58(24):R16016–16019.
- [10] Tan PH, Tang Y, Hu CY, Li F, Wei YL, Cheng HM. *Phys Rev B* 2000;62(8):5186–90.
- [11] Brown SDM, Corio P, Marucci A, Dresselhaus MS, Pimenta MA, Kneipp K. *Phys Rev B* 2000;61(8):R5137–5140.
- [12] Kneipp K, Kneipp H, Corio P, Brown SDM et al. *Phys Rev Lett* 2000;84(15):3470–3.
- [13] Cheng HM, Li F, Sun X, Brown SDM et al. *Chem Phys Lett* 1998;289(5–6):602–10.
- [14] Richter E, Subbaswamy KP. *Phys Rev Lett* 1997;79(14):2738–41.
- [15] Kürti J, Kresse G, Kuzmany H. *Phys Rev B* 1998;58(14):R8869–8872.
- [16] Charlier JC, Lambin P. *Phys Rev B* 1998;57(24):R15037–15040.

# Flexible graphite as a compliant thermoelectric material

Yie Meng Hoi, D.D.L. Chung\*

*Composite Materials Research Laboratory, University at Buffalo, The State University of New York, Buffalo, NY 14260-4400, USA*

Received 3 May 2001; accepted 26 August 2001

*Keywords:* A. Intercalation compounds; Natural graphite; D. Transport properties; Electrical properties

Flexible graphite is a flexible sheet made by compressing a collection of exfoliated graphite flakes (called worms) without a binder [1]. During exfoliation, an intercalated graphite (graphite compound with foreign species called the intercalate between some of the graphite layers) flake expands typically by over 100 times along the *c*-axis. Compression of the resulting worms (like accordions) causes the worms to be mechanically interlocked to one another, so that a sheet is formed without a binder.

Due to the process of exfoliation, flexible graphite has a relatively large specific surface area (e.g. 15 m<sup>2</sup>/g [2]). As a result, flexible graphite is used as an adsorption substrate. Because of the absence of a binder, flexible graphite is essentially entirely graphite (other than the residual amount of intercalate in the exfoliated graphite). As a result, flexible graphite is chemically and thermally resistant, and has a low coefficient of thermal expansion (CTE). Due to

its microstructure involving graphite layers that are preferentially parallel to the surface of the sheet, flexible graphite has high electrical and thermal conductivities in the plane of the sheet. Because graphite layers are somewhat connected perpendicular to the sheet (i.e. the honeycomb microstructure of exfoliated graphite), flexible graphite is electrically and thermally conductive in the direction perpendicular to the sheet (although not as conductive as the plane of the sheet). These in-plane and out-of-plane microstructures result in resilience and impermeability to fluids perpendicular to the sheet. The combination of resilience, impermeability and chemical and thermal resistance makes flexible graphite attractive for use as a gasket material for high temperature or chemically harsh environments.

Gasketing (i.e. packaging, sealing) [3–7] is by far the main application of flexible graphite, which can replace asbestos. Other than gasketing, a number of applications have emerged recently, including adsorption, electromagnetic interference (EMI) shielding, vibration damping, electrochemical applications and stress sensing [1,2,8–10].

\*Corresponding author. Tel.: +1-716-645-2593, ext. 2243; fax: +1-716-645-3875.

*E-mail address:* ddlchung@acsu.buffalo.edu (D.D.L. Chung).